Computers and Geotechnics 70 (2015) 138–149

Contents lists available at ScienceDirect

Computers and Geotechnics

journal homepage: www.elsevier.com/locate/compgeo

Bearing capacity of circular footings over rock mass by using axisymmetric quasi lower bound finite element limit analysis

Manash Chakraborty, Jyant Kumar *

Department of Civil Engineering, Indian Institute of Science, Bangalore 560012, India

ARTICLE INFO

Article history:
Received 25 May 2015
Received in revised form 28 July 2015
Accepted 29 July 2015
Available online 29 August 2015

Keywords:
Bearing capacity
Failure
Foundations
Hoek–Brown criterion
Limit analysis
Finite elements

ABSTRACT

The ultimate bearing capacity of a circular footing, placed over rock mass, is evaluated by using the lower bound theorem of the limit analysis in conjunction with finite elements and nonlinear optimization. The generalized Hoek–Brown (HB) failure criterion, but by keeping a constant value of the exponent, $\alpha = 0.5$, was used. The failure criterion was smoothened both in the meridian and π planes. The nonlinear optimization was carried out by employing an interior point method based on the logarithmic barrier function. The results for the obtained bearing capacity were presented in a non-dimensional form for different values of *GSI*, m_i, $\sigma_{ci}/(\gamma b)$ and q/σ_{ci}. Failure patterns were also examined for a few cases. For validating the results, computations were also performed for a strip footing as well. The results obtained from the analysis compare well with the data reported in literature. Since the equilibrium conditions are precisely satisfied only at the centroids of the elements, not everywhere in the domain, the obtained lower bound solution will be approximate not true.

1. Introduction

The Hoek–Brown (HB) failure criterion [1–4] is a widely accepted yield basis for solving a number of rock mechanics problems, for instance, for (i) carrying out design of underground openings and caverns [5–7], (ii) finding the bearing capacity of foundations over rocks [8–12], and (iii) performing stability analysis of rock slopes [13–15]. The HB criterion is preferred over other alternative yield expressions for rock mass because it provides quite satisfactory answers for predicting the rock failure behaviour by using different input material parameters which can be relatively easily measured by (i) uniaxial testing of rock samples, (ii) mineralogical examination, and (iii) characterization of rock discontinuities. In order to provide a better match between predicted and observed rock behaviour, especially in the case of weak jointed rock mass, the original HB criterion [1] was modified and subsequently a generalized HB criterion [2–4] was proposed. By using the two dimensional HB criterion, a number of investigations [8–15] have been performed for solving a number of plane strain problems, for instance, determining (i) the bearing capacity of strip footing over rocks, and (ii) the stability of rock slopes. No literature, however, seems to exist for determining the bearing capacity of circular footings over rock mass which requires the implementation of the three dimensional (3D) form of the yield criterion. In the present article, the 3D version of the HB criterion has been used. The necessary smoothening of the yield surface has been performed to overcome stress singularities at (i) the apex of the pyramid in the meridian plane, and (ii) the corners of the hexagon in the π plane. The apex of the yield surface in the meridian plane was smoothened by employing a quasi-hyperbolic approximation as was adopted earlier by Merifield et al. [11]. The corners of the hexagon in the π plane were smoothed by using a trigonometric approximation following the approach of Sloan and Booker [16] while dealing with the Mohr Coulomb criterion. For performing the analysis, the lower bound theorem of the limit analysis in combination with finite elements and nonlinear optimization was used. The nonlinear constraint optimization problem was dealt with by using an interior point method (IPM) based on the logarithmic barrier function as proposed by Krabbenhoft and Damkilde [17]. Following this methodology, the bearing capacity of a circular footing placed over rock mass is obtained. The results were presented in a non-dimensional form for different values of *GSI* and m_i; where *GSI* and m_i refer to the non dimensional rock strength parameters. The effects of rock unit weight and surcharge pressure were also exclusively studied. Failure patterns were also been drawn for a

* Corresponding author. Tel.: +91 22933119.
E-mail address: jkumar@civil.iisc.ernet.in (J. Kumar).

http://dx.doi.org/10.1016/j.compgeo.2015.07.015
0266-352X/

number of cases. To validate the results, the bearing capacity of a strip footing over rock mass was also determined and the results obtained were compared with the existing solution of Merifield et al. [11].

2. Hoek–Brown yield criterion

Hoek–Brown yield criterion [1] provides the following empirical relationship between major and minor principle stress (σ_1 and σ_3) for fracture initiation and rock failure.

$$\sigma_1 = \sigma_3 + \left(-m\sigma_1\sigma_{ci} + s\sigma_{ci}^2\right)^{0.5} \tag{1}$$

Hoek and Brown [1] derived this expression by conducting a large number of triaxial tests on several rock samples. In this expression, σ_{ci} defines the uniaxial compressive strength of the intact rock material; the stresses σ_1 and σ_3 are considered as positive when tensile in nature [18]. The variables m and s are dimensionless material parameters; the factor m becomes indirectly analogous to the frictional strength of the rock, and the parameter s, indicates the degree of fracturing of the rock mass. For an intact rock mass, $s = 1$ and for heavily fractured rocks, $s = 0$. For an intact rock mass, the parameter m becomes constant and it depends primarily on the rock type; for highly jointed or fragmented rocks, the parameters m and s decrease with an increase in the degree of fragmentation. The original HB criterion was later modified for the jointed rock mass to provide the following generalized form [3,4]:

$$\sigma_1 = \sigma_3 + \left(-m_b\sigma_1\sigma_{ci}^{(1-\alpha)/\alpha} + s\sigma_{ci}^{1/\alpha}\right)^{\alpha} \tag{2}$$

This criterion is derived on the basis that the rock mass has a number of closely spaced discontinuities but without any preferential plane for shearing. Hence, the isotropic HB criterion is used for assessing the strength characteristics.

In Eq. (2), the term m_b was introduced to account for the broken rock mass. Hoek et al. [4] provided the expression of m_b in terms of (i) m_i, that is, the value of m for an intact rock mass, (ii) geological strength index (GSI) and (iii) the disturbance factor (D). The m_i value depends upon the mineralogy and texture of the intact rock. The parameter GSI accounts for a reduction in rock mass strength subjected to different geological conditions by considering the effect of the geometrical shape of intact rock fragments as well as the condition of joint faces. The factor D considers the disturbance of the rock mass; the value of D varies from 0 for an undisturbed state to 1 for the disturbed rock sample depending on the extent of weathering and blast damage of the rock mass. For performing the present analysis, the parameter D was taken equal to 0. The exponential term α adjusts the curvature of the failure envelope [19]. The relationships among the parameters m_b, s, α, D and GSI, are given herewith [4]:

$$m_b = m_i \exp\left(\frac{GSI - 100}{28 - 14D}\right) \tag{3a}$$

$$s = \exp\left(\frac{GSI - 100}{9 - 3D}\right) \tag{3b}$$

$$\alpha = \frac{1}{2} + \frac{1}{6}\left(\exp\left(\frac{-GSI}{15}\right) - \exp\left(\frac{-20}{3}\right)\right) \tag{3c}$$

The magnitude of GSI was varied in a range from 10 to 100. In this range, the value of α varies between 0.50 and 0.59. For smoothening the generalized HB surface in a π plane, the value of α was taken equal to 0.5 in all the cases; note that the value of α from Eq. (3c) becomes equal to (i) 0.54 for $GSI = 20$, (ii) 0.52 for $GSI = 30$, (ii) 0.51 for $GSI = 50$ and (iii) 0.50 for $GSI = 100$.

In terms of the three stress invariants $(\sigma_m, \overline{\sigma}, \theta)$ as originally proposed by Nayak and Zienkiewicz [20], the major and minor principal stresses can be written as:

$$\sigma_1 = \frac{2}{\sqrt{3}}\overline{\sigma}\sin(\theta + 120^\circ) + \sigma_m \text{ and}$$
$$\sigma_3 = \frac{2}{\sqrt{3}}\overline{\sigma}\sin(\theta - 120^\circ) + \sigma_m \tag{4}$$

By using these expressions, and by assuming $\alpha = 0.5$, the HB yield criterion given in Eq. (2), can be expressed in the following form:

$$f(\sigma) = (2\overline{\sigma}\cos\theta)^2 - m_b\sigma_{ci}\overline{\sigma}\left(\frac{\sin\theta}{\sqrt{3}} - \cos\theta\right) + m_b\sigma_{ci}\sigma_m - s\sigma_{ci}^2 = 0 \tag{5}$$

where $\sigma_m = \frac{1}{3}(\sigma_r + \sigma_z + \sigma_\theta)$; $\quad \overline{\sigma} = \sqrt{\left(s_r^2 + s_z^2 + s_\theta^2\right) + \tau_{rz}^2}$;
$s_i = \sigma_i - \sigma_m \quad (i = r, z, \theta)$

$$-30^\circ \leqslant \theta = \frac{1}{3}\sin^{-1}\left(-\frac{3\sqrt{3}}{2}\frac{J_3}{\overline{\sigma}^3}\right) \leqslant 30^\circ; \quad J_3 = s_r s_z s_\theta - s_\theta\tau_{rz}^2$$

The derivation of the yield function in terms of the stress invariants (Eq. (5)) has been given in Appendix A. It should be mentioned that if the value of α is not taken equal to 0.5, the analytical form of $f(\sigma)$ as expressed by Eq. (5) will not be possible, and hence for the sake of computational convenience, the value of α was taken equal to 0.5 in all the cases. In the three dimensional principal stress space, the HB criterion becomes approximately a pyramid as shown in Fig. 1(a). The edges of this pyramid remain curved, and the projection of the pyramid in a π plane becomes an irregular hexagon. Fig. 1(b) shows the projection of the curved pyramid in a π plane which represents the relationship between $\overline{\sigma}$ and θ (Lode angle) with a constant value of σ_m; the values of θ becomes equal to 30° and −30° correspond to triaxial compression $(\sigma_1 > \sigma_2 = \sigma_3)$ and extension $(\sigma_1 = \sigma_2 > \sigma_3)$ corners, respectively.

3. Smoothening of the HB criterion

While dealing with the nonlinear optimization, the numerical computational procedure requires to have unique values of first and second order derivatives of the yield function $f(\sigma)$ at any point on the yield surface. It, therefore, becomes necessary to obtain a C^2 continuous yield surface to deal with this nonlinear optimization problem. By using the quasi-hyperbolic approach, as given by Merifield et al. [11], the discontinuity at the apex of the yield surface in the meridian plane $(\sigma_m - \overline{\sigma})$ was smoothened. The smoothened HB criterion, that is, without having the sharp apex in the meridian plane, is expressed as:

$$f(\sigma) = \left(2\overset{\leftrightarrow}{\sigma}\cos\theta\right)^2 - m_b\sigma_{ci}\overset{\leftrightarrow}{\sigma}\left(\frac{\sin\theta}{\sqrt{3}} - \cos\theta\right) + m_b\sigma_{ci}\sigma_m - s\sigma_{ci}^2 \tag{6}$$

where (i) $\overset{\leftrightarrow}{\sigma} = \sqrt{\overline{\sigma}^2 + \varepsilon^2}$; (ii) $\varepsilon = \min(\delta, \mu\rho|\rho g(0) + \sqrt{(\rho h(0) + s\sigma_{ci}^2)} = 0)$, and (iii) the constant values of δ and μ are chosen as: $\delta = 10^{-6}$ and $\mu = 10^{-1}$. The yield surface provided in Eq. (6) still possesses discontinuities at the corners of the hexagon in the π plane. The corners of the hexagon in the π plane were smoothened by using a trigonometric approximation, as earlier proposed by Sloan and Booker [16] and was also later followed by Chakraborty and Kumar [21] while dealing with the Mohr–Coulomb criterion. The value of the transition angle (θ_T) has been considered as a basis of transforming the original HB surface to the C^2 continuous modified

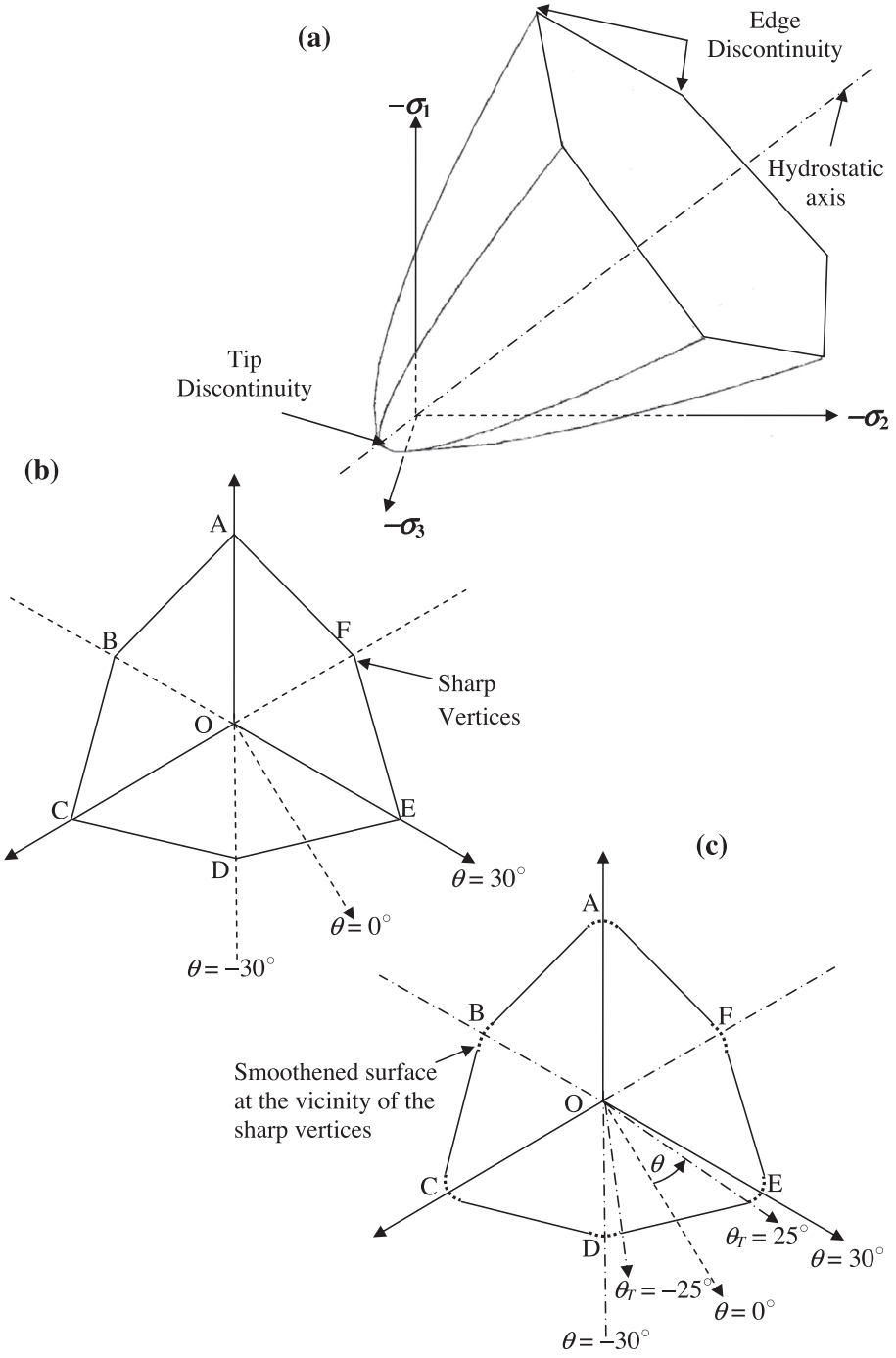

Fig. 1. Representation of the HB yield surface in the (a) 3D principal stress space; (b) π-plane without any smoothening; and (c) π-plane with the smoothening of the vertices.

smoothened yield surface in the vicinity of the sharp corners. The failure criterion is governed by the original HB criterion up to the transition angle θ_T, that is, when $|\theta| < \theta_T$. Beyond the transition angle, that is, $|\theta| \geqslant \theta_T$, the failure criterion is dictated by the modified yield criterion. At the transition point, that is, $|\theta| = \theta_T$, the expression of the modified yield surface is derived by satisfying the condition that the values of the three terms, namely, $\overline{\sigma}, \frac{\partial \overline{\sigma}}{\partial \theta}$ and $\frac{\partial^2 \overline{\sigma}}{\partial \theta^2}$ become the same for the modified as well the original generalized HB yield surface. In order to satisfy the convexity of the yield surface, the values of $\frac{\partial \overline{\sigma}}{\partial \theta}$ obtained at $\theta = \pm 30^\circ$ need to be zero. The following yield function satisfies all the requirements as mentioned earlier.

$$f(\sigma) = m_b \sigma_{ci} \sigma_m - m_b \sigma_{ci} \overset{\leftrightarrow}{\sigma} \left(A + B \sin 3\theta + C \sin^2 3\theta \right) - s\sigma_{ci}^2 \tag{7}$$

By equating the three equations given by the three conditions, the values of A, B and C can be expressed as:

$$A = 8P \cos^2 \theta_T / (Y m_b \sigma_{ci}) - B\langle \psi \rangle \sin 3\theta_T - C \sin^2 3\theta_T \tag{8a}$$

$$B = \sec^3 3\theta_T (k_{12} \cos 6\theta_T - 0.5 k_{11} \langle \psi \rangle \sin 6\theta_T) \tag{8b}$$

$$C = 0.5 \sec^2 3\theta_T (k_{12} \langle \psi \rangle \tan 3\theta_T - k_{11}) \tag{8c}$$

where $P = m_b \sigma_{ci} \sigma_m - s\sigma_{ci}^2$; $Y = m_b \sigma_{ci} R_1 + X$; $Z = m_b \sigma_{ci} R_2 + \frac{1}{2X}(2m_b^2 \sigma_{ci}^2 R_1 R_2 + 16P \sin 2\theta)$

$$R_1 = (\langle\psi\rangle \sin\theta_T/\sqrt{3} - \cos\theta_T);\quad R_2 = (\cos\theta_T/\sqrt{3} + \langle\psi\rangle \sin\theta_T)$$

$$X = (m_b^2\sigma_{ci}^2 R_1^2 - 16P\cos^2\theta)^{0.5}$$

$$k_{11} = \frac{8P}{9Y^2 m_b \sigma_{ci}}\left(k_{10} - \frac{2}{Y}(Z\cos\theta_T + 2Y\langle\psi\rangle \sin\theta_T)^2\right)$$

$$k_{12} = -\frac{8P\cos\theta_T}{3Y^2 m_b \sigma_{ci}}(Z\cos\theta_T + 2Y\langle\psi\rangle \sin\theta_T);\quad k_{14} = 2m_b^2\sigma_{ci}^2 R_1 R_2 + 16P\langle\psi\rangle \sin 2\theta_T$$

$$k_{16} = -\frac{16\sin 2\theta_T m_b \sigma_{ci}}{X^2}k_{13} + \frac{3k_{13}^2 k_{14}}{2X^3};\quad k_{13} = -\frac{1}{X}(8\cos^2\theta_T m_b \sigma_{ci})$$

$$k_{10} = \langle\psi\rangle(Z + k_{13})\sin 2\theta_T + 4Y\sin^2\theta_T + k_{16}\cos^2\theta_T$$

$$\langle\psi\rangle = 1 \text{ if } \theta \geqslant 0^\circ$$

$$= -1 \quad \text{elsewhewre}$$

Finally, the complete form of the smoothened yield function used in the present analysis is expressed as:

$$f(\sigma) = \left(2\overleftrightarrow{\sigma}\cos\theta\right)^2 - m_b\sigma_{ci}\overleftrightarrow{\sigma}\left(\frac{\sin\theta}{\sqrt{3}} - \cos\theta\right) + m_b\sigma_{ci}\sigma_m - s\sigma_{ci}^2 \quad \text{for } |\theta| < \theta_T$$

$$= m_b\sigma_{ci}\sigma_m - m_b\sigma_{ci}\overleftrightarrow{\sigma}\left(A + B\sin 3\theta + C\sin^2 3\theta\right) - s\sigma_{ci}^2 \quad \text{for } |\theta| \geqslant \theta_T \tag{9}$$

It should be mentioned that by using two controlling parameters, namely, ε and θ_T, all the stress singularities present on the yield surface are being removed, and finally a C^2 continuous modified smoothened yield surface is obtained. The modifications are being carried out only at the vicinity of the sharp vertices. The parent HB yield surface can be regained by specifying the values of $\varepsilon = 0$ and $\theta_T = 30^\circ$.

To avoid any ill-conditioning of the modified yield surface, θ_T should not be kept too close to 30° as suggested by Sloan and Booker [16] and Taiebat and Carter [22] while smoothening the Mohr–Coulomb criterion. On the other hand, the accuracy of the solution increases as the value of θ_T is kept closer to 30°. In the present analysis, the value of θ_T was kept equal to 29.50° in all the cases.

4. Determining the bearing capacity of circular foundations over rock mass

A circular rigid footing of radius b is placed over a jointed rock mass with horizontal ground surface which is loaded with surcharge pressure (q). The footing is considered as perfectly rough. The rock mass is assumed to have an uniaxial compressive strength σ_{ci}, geological strength index *GSI*, unit weight γ, and intact rock yield parameter m_i. The rock mass is assumed to be isotropic, perfectly plastic and it obeys an associated flow rule. The footing is subjected to vertical downward load (Q) without having any eccentricity. The ultimate bearing capacity (q_u) of the circular footing is expressed in term of the following expression:

$$q_u = \frac{Q_u}{\pi b^2} = \sigma_{ci}N_\sigma \tag{10}$$

where N_σ is the bearing capacity factor which has been expressed as a function of different input parameters, namely, *GSI*, m_i, $\sigma_{ci}/(\gamma b)$ and q/σ_{ci}. For a weightless rock medium, the bearing capacity factor N_σ is represented as $N_{\sigma o}$.

5. Mesh details and analysis procedure

A planar domain in $r - z$ coordinates, by keeping the axis of symmetry as one of its vertical boundary, was selected for solving the problem. There is no need to consider either the three dimensional angular domain or the angular element. The different boundary conditions on the planar problem domain are specified in Fig. 2(a). The perfectly rough condition between the soil-footing interfaces is modelled by enforcing the requirement that the yield strength between the interface of the footing and underlying rock mass is dictated by the yield strength for the rock medium itself. The depth (H) of the chosen domain is kept equal to the horizontal extent of the domain measured from the footing edge (L_g). The value of L_g is chosen in a fashion such that (i) the plastic shear zones are contained well within chosen domain boundaries, and (ii) an extension of the size of the domain, beyond that chosen, does not affect the magnitude of the collapse load. Considering these issues, the values of L_g is kept between $7b$-$12b$ depending on different rock parameters. The domain is discretized into three nodded constant strain triangular elements. To account for the singularity at the edge of the footing, the sizes of the elements were gradually reduced towards the vicinity of the footing edge. Fig. 2(b) and (c) display the mesh used for evaluating the bearing capacity corresponding to: (a) *GSI* = 90, $m_i = 40$; (b) *GSI* = 10, $m_i = 40$. A zoomed view of the mesh around the footing edge has also been presented in these figures; note that a fan type mesh has been created near the edge of the footing. It was assured that any further increment in the number of the elements near the footing edge than that chosen for the finalization of the results does not cause any significant change in the magnitude of the collapse load.

To obtain the lower bound solution it is required to obtain a statically admissible stress field which satisfies equilibrium conditions, stress discontinuity conditions, stress boundary conditions and further it should not violate the yield criterion. The equations of the statical equilibrium condition in an axisymmetric analysis are defined in terms of the cylindrical coordinates and these equations are expressed as:

$$\frac{\partial\sigma_r}{\partial r} + \frac{\partial\tau_{rz}}{\partial z} + \frac{\sigma_r - \sigma_\theta}{r} = 0 \text{ and } \frac{\partial\sigma_z}{\partial z} + \frac{\partial\tau_{rz}}{\partial r} + \frac{\tau_{rz}}{r} = \gamma \tag{11}$$

It needs to be mentioned that in the present analysis, the equilibrium conditions are satisfied only at the centroids of the elements not everywhere. Therefore, the obtained solution will be approximate not strictly true. Unlike the displacement-based finite element analysis, in the present case each node is assumed to be associated with a particular element and the interface boundary between two adjacent elements is taken as the line of the stress discontinuity. Normal and shear stresses (σ_n and τ_{nt}) are always kept continuous across any chosen stress discontinuity line. For instance, if 1–3 and 2–4 are the two stress discontinuity lines associated with two triangular elements, a and b; nodes (1, 2) and (3, 4) sharing the same coordinates, then the basic stress discontinuity requirements can be expressed by the equations:

$$\sigma_{n,1}^a = \sigma_{n,2}^b;\ \tau_{nt,1}^a = \tau_{nt,2}^b = \text{ and } \sigma_{n,3}^a = \sigma_{n,4}^b;\ \tau_{nt,3}^a = \tau_{nt,4}^b \tag{12}$$

This satisfies the equilibrium condition along the discontinuity boundaries. The stress conditions defined along the specified boundary lines need to be satisfied. By integrating the vertical normal stresses along the footing-soil interface, the objective function was accordingly defined by the following expression:

$$Q_u = 2\pi\int_{L_s}\sigma_n r ds = \boldsymbol{b}^T\boldsymbol{\sigma} \tag{13}$$

where (i) $\boldsymbol{b}$ defines a vector containing coefficient terms of the objective function; and (ii) $\boldsymbol{\sigma}$ implies global unknown stress vector. For a complete description on the formation of the equality constraints and the objective function, one can refer to the papers of Kumar and Khatri [23] and Sloan [24]. The optimization problem is finally expressed in the following form:

$$\text{Maximize}: \ \boldsymbol{b}^T\boldsymbol{\sigma};\quad \text{Subjected to}: \ \boldsymbol{A_{eq}}\boldsymbol{\sigma} = \boldsymbol{B_{eq}} \text{ and } f(\boldsymbol{\sigma}) \leqslant 0 \tag{14}$$

where $\boldsymbol{A_{eq}}$ and $\boldsymbol{B_{eq}}$ are the coefficient matrix and the right-hand side vector of equality constraints, respectively. This nonlinear optimization problem was solved by using an interior point method (IPM)

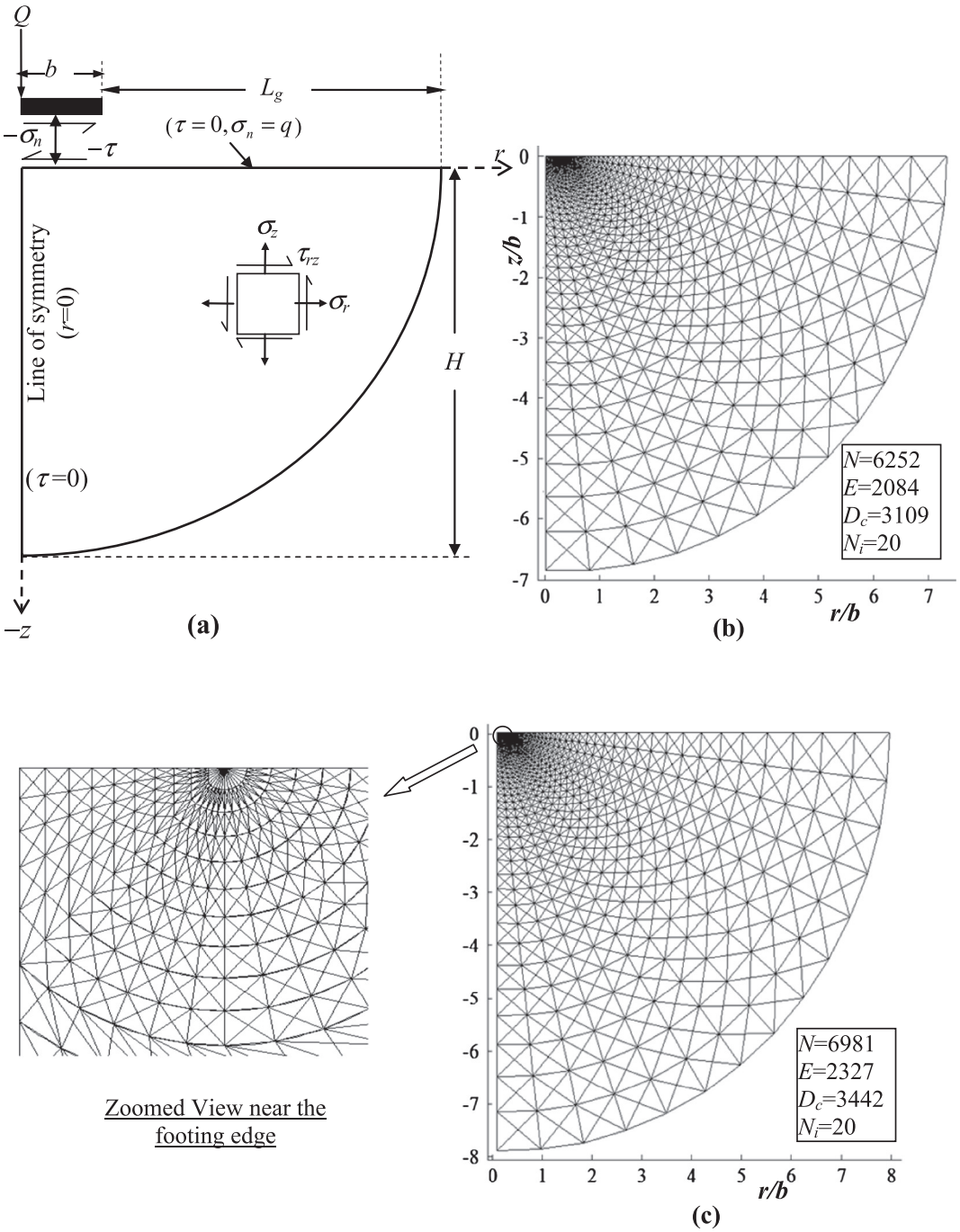

Fig. 2. (a) Chosen domain and stress boundary conditions for a circular footing; (b) the chosen mesh for *GSI* = 90, $m_i = 40$; and (c) the mesh for *GSI* = 10, $m_i = 40$.

based on the logarithmic barrier function as described in the study of Chakraborty and Kumar [21]. The search direction is obtained by using the modified Newton's method and along the search direction, the step size is calculated and the unknown variables are accordingly updated; this iteration technique is followed till the following convergence criteria is attained:

$$\max(f(\boldsymbol{\sigma})) \leqslant 10^{-5}; \quad abs\left((\boldsymbol{b}^T\boldsymbol{\sigma})^k - (\boldsymbol{b}^T\boldsymbol{\sigma})^{k-1}\right) < 10^{-5}; \text{ and } norm(\boldsymbol{A_{eq}\sigma} - \boldsymbol{B_{eq}}) < 10^{-10} \tag{15}$$

where k denotes the iteration number. While performing the nonlinear optimization, it is needed to obtain gradient and hessian matrices of the yield function. The gradient and the hessian matrices of the modified HB yield function $(f(\sigma))$ are presented in Appendix B.

6. Results and discussions

The computations have been performed by varying the value of *GSI* from 10 to 100 corresponding to different values of m_i, namely, 1, 5, 10, 20, 30, 35 and 40. For a weightless medium, Fig. 3(a) shows the variation of $N_{\sigma o}$ with m_i for different values of *GSI*. It is observed that for a given value of *GSI*, the magnitude of $N_{\sigma o}$ increases continuously with an increase in m_i. The rate of increase of $N_{\sigma o}$ with m_i decreases continuously with an increase in the value of m_i. The value of $N_{\sigma o}$ also increases further with an increase in the value of *GSI*.

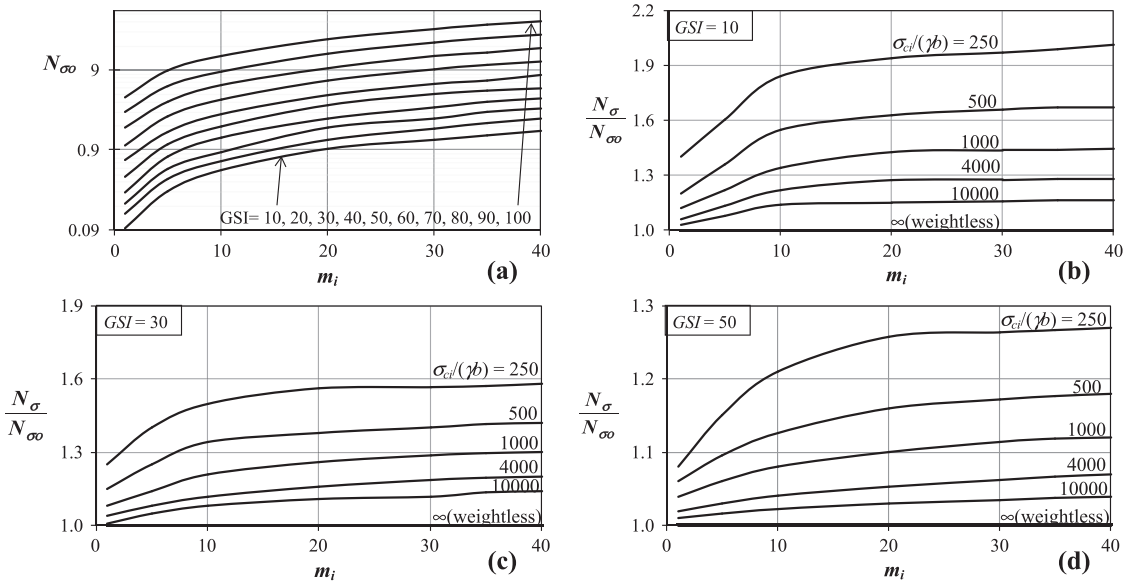

Fig. 3. (a) The variation of $N_{\sigma o}$ with m_i and *GSI*; (b) the variation of $N_\sigma/N_{\sigma o}$ with m_i and $\sigma_{ci}/(\gamma b)$ for *GSI* = 10; (c) the variation of $N_\sigma/N_{\sigma o}$ with m_i and $\sigma_{ci}/(\gamma b)$ for *GSI* = 30; and (d) the variation of $N_\sigma/N_{\sigma o}$ with m_i and $\sigma_{ci}/(\gamma b)$ for GSI = 50.

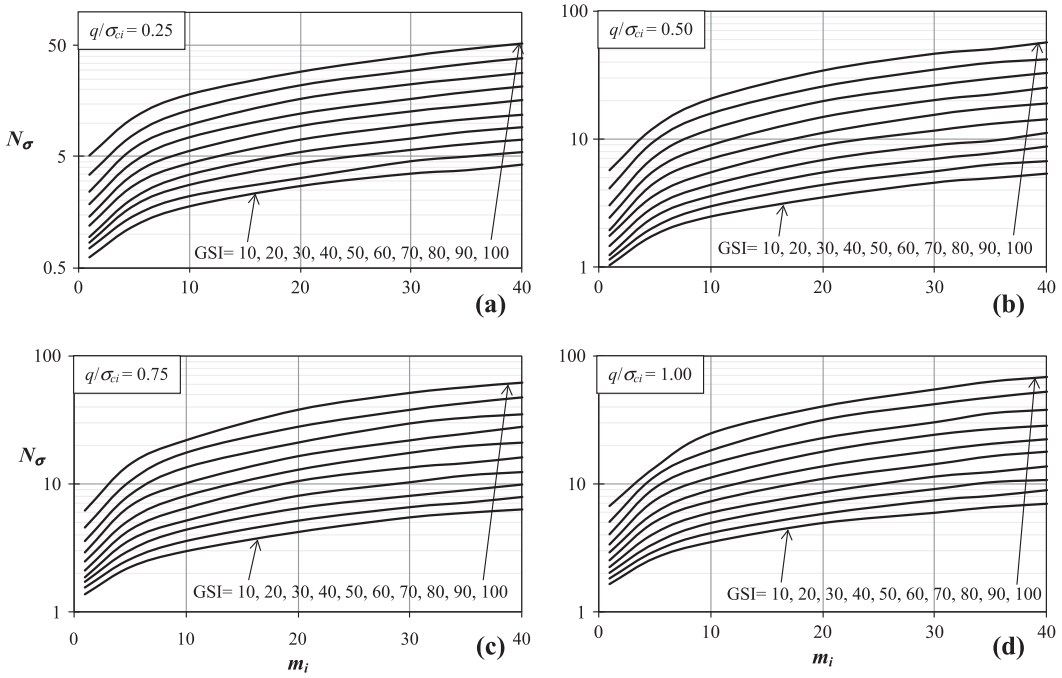

Fig. 4. For $\sigma_{ci}/(\gamma b) = 250$, the variation of N_σ with m_i and *GSI* for (a) $q/\sigma_{ci} = 0.25$; (b) $q/\sigma_{ci} = 0.50$; (c) $q/\sigma_{ci} = 0.75$; and (d) $q/\sigma_{ci} = 1$.

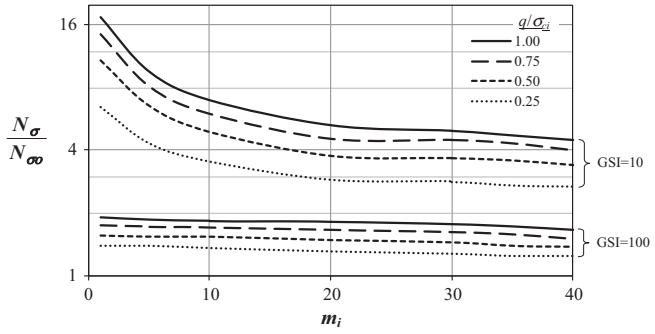

Fig. 5. For $\sigma_{ci}/(\gamma b) = 250$, the variation of $N_\sigma/N_{\sigma 0}$ with m_i for different combinations of GSI and q/σ_{ci}.

Fig. 3(b)–(d) present the effect of unit weight on the bearing capacity for different values of *GSI* and m_i. This is presented in terms of the variation of a ratio, $N_\sigma/N_{\sigma o}$, with changes in m_i for different values of $\sigma_{ci}/(\gamma b)$ which was varied between 250 and 10,000; note that the factor N_σ is associated with an inclusion of rock unit weight. It can be noted that the value of the ratio $N_\sigma/N_{\sigma o}$ increases continuously with a decrease in the magnitude of $\sigma_{ci}/(\gamma b)$; the value of N_σ becomes simply equal to $N_{\sigma o}$ for $\sigma_{ci}/(\gamma b) = \infty$, that is, when γ = 0. The effect of unit weight becomes more pronounced for lower values of *GSI*; for instance for $\sigma_{ci}/(\gamma b) = 250$ and $m_i = 20$, the value of N_σ has been found to be approximately 1.95, 1.55 and 1.25 times $N_{\sigma o}$ corresponding to *GSI* = 10, 30 and 50, respectively. It is noted that if the *GSI* value

Table 1
For a strip footing on rock mass, a comparison of the bearing capacity factor obtained from the present analysis with the solution of Merifield et al. [11] for different values of *GSI* and m_i.

GSI	m_i	Present solution	Merifield et al. [11]	*GSI*	m_i	Present solution	Merifield et al. [11]
10	1	0.014	0.015	60	1	0.461	0.465
	5	0.040	0.042		5	1.009	1.013
	10	0.075	0.077		10	1.567	1.597
	20	0.151	0.156		20	2.600	2.667
	30	0.230	0.238		30	3.592	3.644
	35	0.276	0.288		35	4.049	4.186
20	1	0.042	0.044	70	1	0.761	0.765
	5	0.117	0.119		5	1.571	1.582
	10	0.204	0.209		10	2.415	2.444
	20	0.377	0.389		20	3.978	4.012
	30	0.567	0.575		30	5.437	5.491
	35	0.662	0.670		35	6.036	6.068
30	1	0.090	0.092	80	1	1.251	1.260
	5	0.230	0.235		5	2.456	2.473
	10	0.388	0.397		10	3.712	3.745
	20	0.701	0.713		20	5.983	6.040
	30	1.015	1.022		30	8.085	8.195
	35	1.182	1.193		35	9.118	9.242
40	1	0.161	0.165	90	1	2.065	2.083
	5	0.399	0.401		5	3.846	3.881
	10	0.647	0.659		10	5.724	5.758
	20	1.138	1.149		20	9.086	9.125
	30	1.616	1.630		30	12.198	12.270
	35	1.846	1.873		35	13.618	13.794
50	1	0.272	0.281	100	1	3.433	3.461
	5	0.631	0.644		5	6.095	6.124
	10	1.028	1.037		10	8.798	8.896
	20	1.739	1.765		20	13.789	13.847
	30	2.406	2.467		30	18.398	18.444
	35	2.766	2.817		35	20.587	20.668

Note: The generalized Hoek–Brown yield criterion has been used. Bearing capacity factor, $N_\sigma = q_u/\sigma_{ci}$.

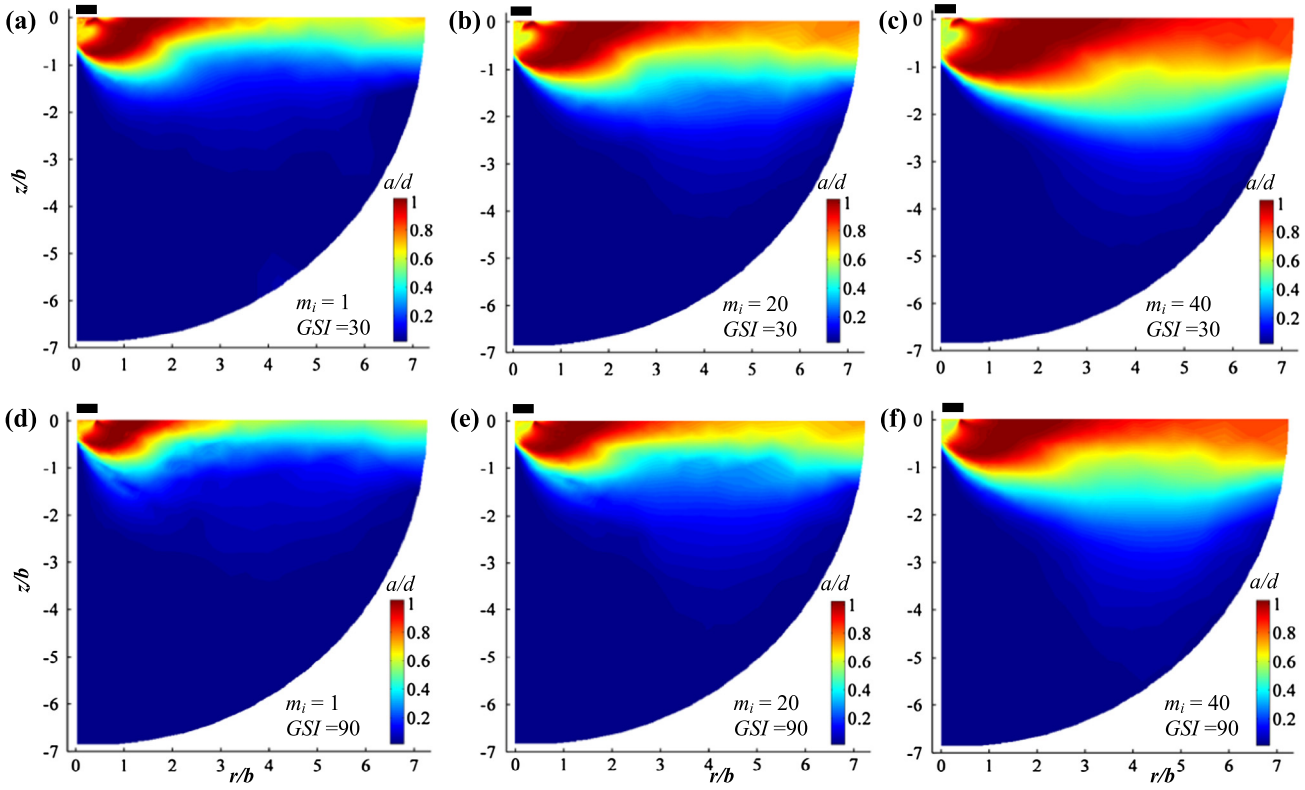

Fig. 6. Failure patterns for a weightless rock medium without any surcharge pressure for: (a) *GSI* = 30, $m_i = 1$; (b) *GSI* = 30, $m_i = 20$; (c) *GSI* = 30, $m_i = 40$; (d) *GSI* = 90, $m_i = 1$; (e) *GSI* = 90, $m_i = 20$; and (f) *GSI* = 90, $m_i = 40$.

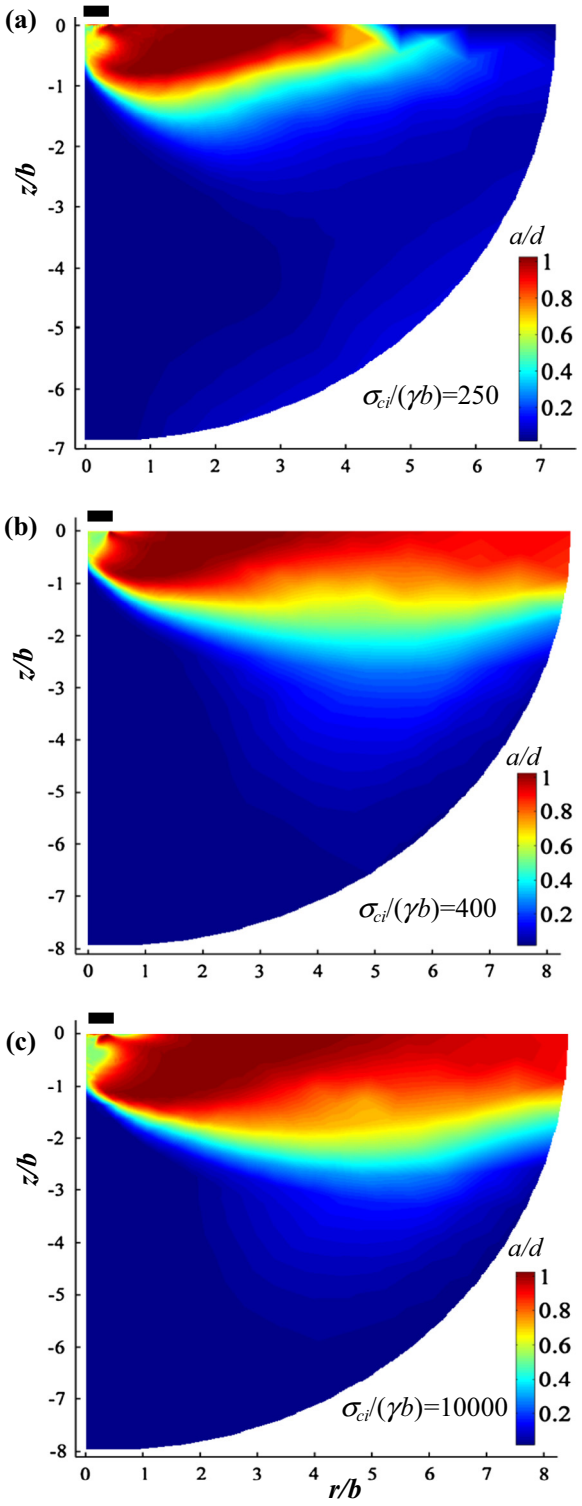

Fig. 7. With $GSI = 10$, $m_i = 40$ and $q = 0$, failure patterns for (a) $\sigma_{ci}/(\gamma b) = 250$; (b) $\sigma_{ci}/(\gamma b) = 4000$; and (c) $\sigma_{ci}/(\gamma b) = 10,000$.

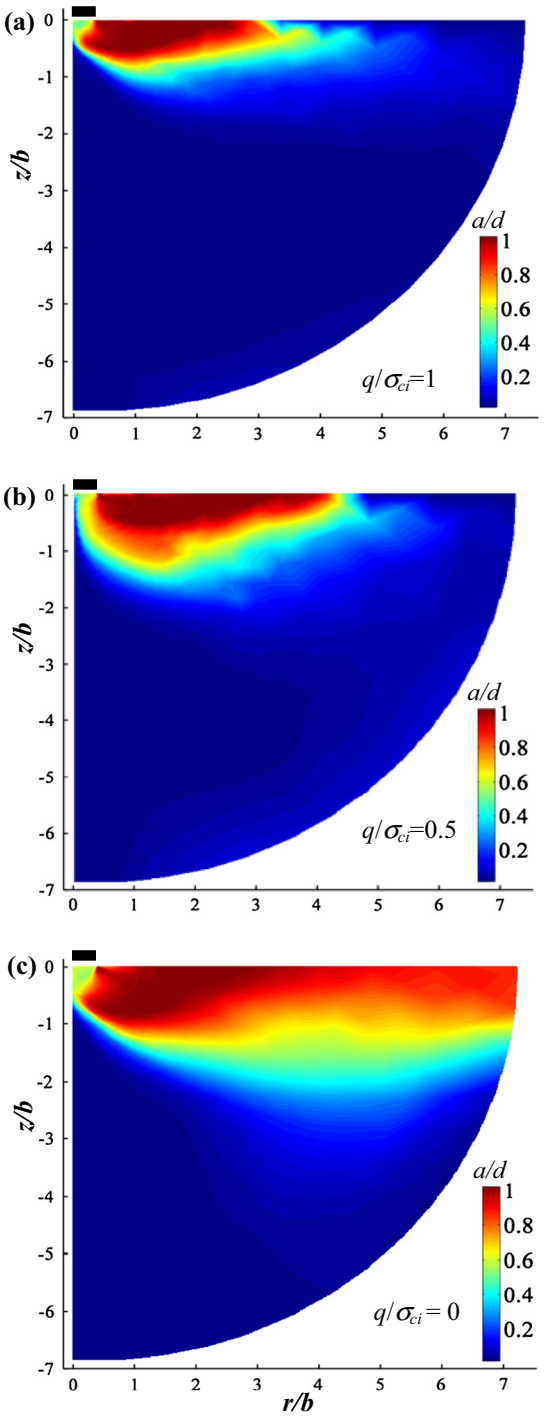

Fig. 8. With $GSI = 50$, $m_i = 40$ and $\sigma_{ci}/(\gamma b) = 250$, failure patterns for (a) $q/\sigma_{ci} = 1$; (b) $q/\sigma_{ci} = 0.5$; and (c) $q/\sigma_{ci} = 1.0$.

of the rock mass exceeds approximately 50, hardly any increment in the bearing capacity occurs with an inclusion of the rock unit weight.

Fig. 4 displays the effect of surcharge pressure (q) on the factor N_σ. Four different values of non-dimensional surcharge pressure term (q/σ_{ci}), namely, 0.25, 0.50, 0.75 and 1, were chosen. While determining the effect of surcharge pressure, the value of $\sigma_{ci}/(\gamma b)$ was kept equal to 250 in all the cases. The results in the presence of surcharge pressure were obtained for different values of GSI and m_i. Note that with the same values of GSI and m_i, the magnitude of N_σ increases continuously with an increase in the value of q/σ_{ci}. Fig. 5 depicts the ratio of the bearing capacity with and without surcharge pressure for different values of m_i corresponding to two different GSI values, namely, 10 and 100. It can be observed that the increase in the bearing capacity with an inclusion of the

surcharge pressure becomes quite higher for lower values of m_i and the corresponding rate of increase of N_σ with q reduces with an increase in m_i. With the same value of m_i, the increase in the bearing capacity due to a given surcharge becomes greater for lower values of *GSI*. For instance, for $m_i = 1$ and for $q/\sigma_{ci} = 0.25$, corresponding to the values of *GSI* = 10 and 100, the magnitude of N_σ becomes 6.47 and 1.41 times the corresponding values of N_σ without any surcharge pressure, respectively.

7. Validation of the results

In order to validate the present computational procedure, the chosen methodology was first used to obtain the $N_{\sigma o}$ value for a strip footing placed over rock mass; it needs to be mentioned that at present there is no solution available in literature for a circular footing over rock mass. The 3D generalized HB criterion with a varying exponent α and a constant lode angle ($\theta = 0^\circ$) was used for obtaining the plane strain solution [25]. The yield function, gradient and hessian are defined in x–y Cartesian coordinate system and can be expressed as follows:

$$\text{Yield Function}: \ f(\sigma) = m_b\sigma_{ci}^{(1-\alpha)/\alpha}(\sigma_m + \overleftrightarrow{\sigma}) + (2\overleftrightarrow{\sigma})^{1/\alpha} - s\sigma_{ci}^{1/\alpha} = 0 \qquad (16)$$

Here the stress invariant are expressed as:

$$\sigma_m = 0.5(\sigma_x + \sigma_y); \quad \overline{\sigma} = \sqrt{0.5(s_x^2 + s_y^2) + \tau_{xy}^2};$$
$$s_i = (\sigma_i - \sigma_m) \ (i = x, y) \qquad (17)$$

$$\text{Gradient}: \quad \Delta f = \frac{\partial f}{\partial \boldsymbol{\sigma}} = C_1\frac{\partial \sigma_m}{\partial \boldsymbol{\sigma}} + C_2\frac{\partial \overline{\sigma}}{\partial \boldsymbol{\sigma}} \qquad (18)$$

$$\text{where } C_1 = \frac{\partial f}{\partial \sigma_m} = m_b\sigma_{ci}^{(1-\alpha)/\alpha}; \quad C_2 = \frac{\partial f}{\partial \overline{\sigma}} = m_b\sigma_{ci}^{(1-\alpha)/\alpha}\frac{\overline{\sigma}}{\overleftrightarrow{\sigma}} + (2)^{1/\alpha}\frac{\overline{\sigma}}{\alpha}(\overleftrightarrow{\sigma})^{(1-2\alpha)/\alpha}$$

$$\text{Hessian}: \quad \Delta^2 f = \frac{\partial^2 f}{\partial \boldsymbol{\sigma}} = \frac{\partial C_2}{\partial \boldsymbol{\sigma}}\frac{\partial \overline{\sigma}}{\partial \boldsymbol{\sigma}} + C_2\frac{\partial^2 \overline{\sigma}}{\partial \boldsymbol{\sigma}^2} \qquad (19)$$

$$\frac{\partial C_2}{\partial \boldsymbol{\sigma}} = m_b\sigma_{ci}^{(1-\alpha)/\alpha}\frac{\varepsilon^2}{\overleftrightarrow{\sigma}^3} + \frac{(2)^{1/\alpha}}{\alpha}\left(\frac{\overline{\sigma}^2(1-2\alpha)}{\alpha}\overleftrightarrow{\sigma}^{(1-4\alpha)/\alpha} + \overleftrightarrow{\sigma}^{(1-2\alpha)/\alpha}\right)$$

Note that it is not required to assign the value of α to be 0.5 for the plane strain analysis as the lode angle is fixed and there is no need to smoothen the yield criterion in the π-plane.

The factor $N_{\sigma o}$ was obtained for different values of *GSI* varying from 10 to 100 corresponding to six different values of m_i, namely, 1, 5, 10, 20, 30 and 35. Table 1 shows a comparison between the present $N_{\sigma o}$ values and that reported by Merifield et al. [11]. It needs to be mentioned that the $N_{\sigma o}$ value reported by Merifield et al. [11] was the average of the corresponding lower and upper bound solutions. In all the cases, the values of $N_{\sigma o}$ obtained by Merifield et al. [11] are found to be marginally greater than the present solution; the upper bound solution will obviously provide a slightly greater bearing capacity as compared to the corresponding lower bound solution. Note that the difference between the solutions remains quite insignificant in all the cases which validates the computational procedure followed in this research work. The plane strain yield criterion is the reduced version of the 3D yield criterion; the comparisons of the results for a strip footing, therefore, validates the present computational procedure for an equivalent plane strain problem.

8. Failure patterns

At a given point, in order to check the proximity of the established stress state to that at yield, the failure patterns' figures were drawn on the basis of a ratio, a/d; where for a given point, the parameter a defines the value of $\overleftrightarrow{\sigma}$ as determined from the solution, and d implies the value of $\overleftrightarrow{\sigma}$ which is required to generate the yield state for the same value of σ_m. The value of $\overleftrightarrow{\sigma}$ at failure can be obtained by using Eq. (9) by enforcing $f(\sigma) = 0$; except the value of the variable $\overleftrightarrow{\sigma}$, the values of all the other variables were kept the same as determined from the established solution. The value of the a/d ratio shows the closeness of each point towards the failure state; if the value of a/d becomes equal to 1, then the stress state will be at failure. Fig. 6 shows the failure patterns for a weightless rock mass, with $q = 0$, with different combinations of *GSI* and m_i. The plastic zones in these figures can be easily identified depending upon the value of a/d. With *GSI* = 10, $m_i = 40$ and $q = 0$, Fig. 7 displays failure patterns for three different values of $\sigma_{ci}/(\gamma b)$, namely, 250, 4000 and 10,000. For *GSI* = 50, $m_i = 40$ and $\sigma_{ci}/(\gamma b) = 250$, Fig. 8 shows the failure patterns for three different values of q/σ_{ci}, namely, 0,0.5 and 1. It can be noted from all the failure pattern figures, a non plastic region appears to develop below the footing base in all the cases. Starting from the tip of this non-plastic region, a plastic zone spreads gradually towards ground surface. The outer boundary of this plastic region becomes curvilinear in nature. At any point on this curvilinear boundary, the radial distance from the footing edge increases continuously as the point is taken away from the footing base. The extent of the plastic domain at ground surface increases with an increase in the value of $\sigma_{ci}/(\gamma b)$ but reduces, on the other hand, with an increase in the value of q/σ_{ci}. The extent of the plastic domain surface increases with an increase in the value of m_i. For greater values of *GSI*, the extent of the plastic domain was found to become smaller. The depth of the plastic domain in different cases, as illustrated in Figs. 6–8, was found to vary roughly between 0.6b and 1.4b.

9. Conclusions

Based on the quasi lower bound limit analysis, in conjunction with finite elements and non-linear optimization, a methodology has been given for determining the bearing capacity of a circular footing over rock mass. The yielding of the rock mass is assumed to be governed by the Hoek–Brown yield criterion. The failure criterion was smoothened both in π and meridian planes. The bearing capacity factors have been computed for different combinations of *GSI* and m_i. The value of (i) *GSI* was varied from 10 to 100, and (ii) m_i from 1 to 40. The results were also obtained for different values of $\sigma_{ci}/(\gamma b)$ and q/σ_{ci} to incorporate the effects of unit weight and surcharge pressure. The magnitude of N_σ was found to increase continuously with increases in the values of *GSI*, m_i and q/σ_{ci}. On the other hand, an increase in the value of $\sigma_{ci}/(\gamma b)$ leads to a reduction in N_σ. The effect of $\sigma_{ci}/(\gamma b)$ on N_σ was found to be more substantial for smaller values of *GSI*. The failure pattern figures generated from the analysis clearly reveal that the size of the plastic zone increases with an increase in the values of $\sigma_{ci}/(\gamma b)$ but reduces with an increase in the value of q/σ_{ci}. Necessary validation of the results was presented by performing the analysis for a strip footing as well to illustrate the correctness of the computational procedure. The solution generated from the present analysis will

be approximate since the equilibrium conditions are satisfied only at the centroids of the elements not throughout the domain.

Appendix A. Derivation of the HB yield function in stress invariant form

By using $\alpha = 0.5$, the generalized form of the HB criterion (Eq. (2)) can be written as:

$$\sigma_1 = \sigma_3 + \left(-m_b\sigma_1\sigma_{ci} + s\sigma_{ci}^2\right)^{0.5}$$
$$\Rightarrow (\sigma_1 - \sigma_3)^2 = \left(-m_b\sigma_1\sigma_{ci} + s\sigma_{ci}^2\right) \tag{A.1}$$

From Eq. (4), $(\sigma_1 - \sigma_3)$ can be written as, $2\overline{\sigma}\cos\theta$. Therefore, Eq. (A.1) can be written as,

$$(2\overline{\sigma}\cos\theta) = \left(-m_b\sigma_{ci}\left(\frac{2}{\sqrt{3}}\overline{\sigma}\sin(\theta+120^\circ) + \sigma_m\right) + s\sigma_{ci}^2\right)^{0.5}$$

$$(2\overline{\sigma}\cos\theta)^2 = \left(-m_b\sigma_{ci}\left(\frac{2}{\sqrt{3}}\overline{\sigma}(\sin\theta\cos120^\circ + \cos\theta\sin120^\circ) + \sigma_m\right) + s\sigma_{ci}^2\right)$$
$$= \left(m_b\sigma_{ci}\overline{\sigma}\left(\frac{\sin\theta}{\sqrt{3}} - \cos\theta\right) - m_b\sigma_{ci}\sigma_m + s\sigma_{ci}^2\right)$$

$$\therefore f(\sigma) = (2\overline{\sigma}\cos\theta)^2 - m_b\sigma_{ci}\overline{\sigma}\left(\frac{\sin\theta}{\sqrt{3}} - \cos\theta\right) + m_b\sigma_{ci}\sigma_m - s\sigma_{ci}^2 = 0 \tag{A.2}$$

Appendix B. Gradient and hessian of HB yield function

B.1. Gradient of the yield function

$$\nabla f = \frac{\partial f}{\partial \boldsymbol{\sigma}} = C_1\frac{\partial\sigma_m}{\partial\boldsymbol{\sigma}} + C_2\frac{\partial\overline{\sigma}}{\partial\boldsymbol{\sigma}} + C_3\frac{\partial J_3}{\partial\boldsymbol{\sigma}} \tag{B.1}$$

(i) For $|\theta| < \theta_T, C_1 = \frac{\partial f}{\partial\sigma_m} = m_b\sigma_{ci}$

$$C_2 = \frac{\partial f}{\partial\overline{\sigma}} - \frac{\tan3\theta}{\overline{\sigma}}\frac{\partial f}{\partial\theta} = \frac{\overline{\sigma}}{\overleftrightarrow{\sigma}}k_1 + \frac{\tan3\theta}{\overline{\sigma}}k_2$$

$$C_3 = -\frac{\sqrt{3}}{2}\frac{1}{\cos3\theta}\frac{1}{\overline{\sigma}^3}\frac{\partial f}{\partial\theta} = \frac{\sqrt{3}}{2\cos3\theta\overline{\sigma}^3}k_2$$

where $k_1 = -m_b\sigma_{ci}\left(\frac{\sin\theta}{\sqrt{3}} - \cos\theta\right) + (8\overleftrightarrow{\sigma}\cos^2\theta)$

$$k_2 = m_b\sigma_{ci}\overleftrightarrow{\sigma}\left(\frac{\cos\theta}{\sqrt{3}} + \sin\theta\right) + (4\overleftrightarrow{\sigma}^2\sin2\theta)$$

$$\frac{\partial\sigma_m}{\partial\boldsymbol{\sigma}} = \frac{1}{3}\begin{Bmatrix}1\\1\\0\\1\end{Bmatrix};\quad \frac{\partial\overline{\sigma}}{\partial\boldsymbol{\sigma}} = \frac{1}{2\overline{\sigma}}\begin{Bmatrix}s_r\\s_z\\2\tau_{rz}\\s_\theta\end{Bmatrix};\quad \frac{\partial J_3}{\partial\boldsymbol{\sigma}} = \begin{bmatrix}s_zs_\theta + \frac{\overline{\sigma}^2}{3}\\s_rs_\theta + \frac{\overline{\sigma}^2}{3}\\-2s_\theta\tau_{rz}\\s_zs_r - \tau_{rz}^2 + \frac{\overline{\sigma}^2}{3}\end{bmatrix}$$

(ii) For $|\theta| \geqslant \theta_T, C_1 = m_b\sigma_{ci} - m_b\sigma_{ci}\overleftrightarrow{\sigma}(k_{24} + k_{25}\sin3\theta + k\ 26\sin^2 3\theta)$

$$C_2 = -m_b\sigma_{ci}\left(A + B\sin3\theta + C\sin^2 3\theta\right)\frac{\overline{\sigma}}{\overleftrightarrow{\sigma}} + \frac{3\tan3\theta}{\overline{\sigma}}m_b\sigma_{ci}\overleftrightarrow{\sigma}(B\cos3\theta + C\sin6\theta)$$

$$C_3 = \frac{3\sqrt{3}m_b\sigma_{ci}\overleftrightarrow{\sigma}}{2\overline{\sigma}^3}(B + 2C\sin3\theta)$$

where $k_{18} = \langle\psi\rangle\sin2\theta_T(k_{15} + k_{17}) + 4k_{13}\sin^2\theta_T + k_{16}\cos^2\theta_T$

$$k_{19} = \frac{m_b\sigma_{ci}}{Y^2} - \frac{2Pk_{13}}{Y^3};\quad k_{20} = \frac{m_b\sigma_{ci}}{Y^3} - \frac{3Pk_{13}}{Y^4}$$

$$k_{21} = 2(Z\cos\theta_T + 2Y\langle\psi\rangle\sin\theta_T)(k_{15}\cos\theta_T + 2k_{13}\langle\psi\rangle\sin\theta_T)$$

$$k_{22} = \left(\frac{8}{9m_b\sigma_{ci}}\left(k_{10}k_{19} - 2k_{20}(Z\cos\theta_T + 2Y\langle\psi\rangle\sin\theta_T)^2\right) + \frac{8P}{9Y^2m_b\sigma_{ci}}(k_{18} - \frac{2}{Y}k_{21})\right)$$

$$k_{23} = -\frac{8k_{19}\cos\theta_T}{3m_b\sigma_{ci}}(Z\cos\theta_T + 2Y\langle\psi\rangle\sin\theta_T) - \frac{8P\cos\theta_T}{3Y^2m_b\sigma_{ci}}(k_{15}\cos\theta_T + 2k_{13}\langle\psi\rangle\sin\theta_T)$$

$$k_{24} = \frac{\partial A}{\partial\sigma_m} = \frac{8\cos^2\theta_T}{m_b\sigma_{ci}}\left(\frac{m_b\sigma_{ci}}{Y} - \frac{Pk_{13}}{Y^2}\right) - \left(\frac{\cos6\theta_T\sin3\theta_T}{\cos^3 3\theta_T} + 0.5\tan^3 3\theta_T\right)k_{23} + 1.5\tan^2 3\theta_Tk_{22}$$

$$k_{25} = \frac{\partial B}{\partial\sigma_m} = \sec^3 3\theta_T(k_{23}\cos6\theta_T - 0.5k_{22}\langle\psi\rangle\sin6\theta_T)$$

$$k_{26} = \frac{\partial C}{\partial\sigma_m} = 0.5\sec^3 3\theta_T(k_{23}\langle\psi\rangle\tan3\theta_T - k_{22})$$

B.2. Hessian of the yield function

$$\nabla^2 f = \frac{\partial C_2}{\partial\boldsymbol{\sigma}}\frac{\partial\overline{\sigma}}{\partial\boldsymbol{\sigma}} + C_2\frac{\partial^2\overline{\sigma}}{\partial\boldsymbol{\sigma}^2} + \frac{\partial C_3}{\partial\boldsymbol{\sigma}}\frac{\partial J_3}{\partial\boldsymbol{\sigma}} + C_3\frac{\partial^2 J_3}{\partial\boldsymbol{\sigma}^2} \tag{B.2}$$

$$\frac{\partial C_2}{\partial\boldsymbol{\sigma}} = \frac{\partial C_2}{\partial\overline{\sigma}}\frac{\partial\overline{\sigma}}{\partial\boldsymbol{\sigma}} + \frac{\partial C_2}{\partial\theta}\frac{\partial\theta}{\partial\boldsymbol{\sigma}}$$

$$\frac{\partial C_3}{\partial\boldsymbol{\sigma}} = \frac{\partial C_3}{\partial\overline{\sigma}}\frac{\partial\overline{\sigma}}{\partial\boldsymbol{\sigma}} + \frac{\partial C_3}{\partial\theta}\frac{\partial\theta}{\partial\boldsymbol{\sigma}}$$

(i) For $|\theta| < \theta_T, \frac{\partial C_2}{\partial\overline{\sigma}} = \left(\frac{\overline{\sigma}^2}{\overline{\sigma}^3}\right)k_1 - \frac{\tan3\theta}{\overline{\sigma}^2}k_2 + \left(\frac{\overline{\sigma}}{\overline{\sigma}}\right)^2k_3 + \frac{\tan3\theta}{\overline{\sigma}}k_4 = k_6$

$$\frac{\partial C_2}{\partial\theta} = -\left(\frac{\overline{\sigma}}{\overleftrightarrow{\sigma}}\right)k_4 + \frac{\tan3\theta}{\overline{\sigma}}k_5 + \frac{3\sec^2 3\theta}{\overline{\sigma}}k_2 = k_7$$

$$\frac{\partial C_3}{\partial\overline{\sigma}} = \frac{\sqrt{3}}{2\cos3\theta\overline{\sigma}^3}\left(\frac{-3k_2}{\overline{\sigma}} - \frac{\overline{\sigma}}{\overleftrightarrow{\sigma}}k_4\right) = k_8$$

$$\frac{\partial C_3}{\partial\theta} = \frac{\sqrt{3}}{2\cos3\theta\overline{\sigma}^3}(3k_2\tan3\theta + k_5) = k_9$$

where $k_3 = 8\cos^2\theta; k_4 = 4\overleftrightarrow{\sigma}\sin2\theta + \frac{k_2}{\overleftrightarrow{\sigma}}; k_5 = -m_b\sigma_{ci}\overleftrightarrow{\sigma}\left(\frac{\sin\theta}{\sqrt{3}} - \cos\theta\right) + 8\overleftrightarrow{\sigma}^2\cos2\theta$

$$\nabla^2 f = \frac{\partial C_2}{\partial\boldsymbol{\sigma}}\frac{\partial\overline{\sigma}}{\partial\boldsymbol{\sigma}} + C_2\frac{\partial^2\overline{\sigma}}{\partial\boldsymbol{\sigma}^2} + \frac{\partial C_3}{\partial\boldsymbol{\sigma}}\frac{\partial J_3}{\partial\boldsymbol{\sigma}} + C_3\frac{\partial^2 J_3}{\partial\boldsymbol{\sigma}^2}$$

(ii) For $|\theta| \geqslant \theta_T, \frac{\partial C_1}{\partial\sigma_m} = -m_b\sigma_{ci}\overleftrightarrow{\sigma}\left(k_{41} + k_{42}\sin3\theta + k_{43}\sin^2 3\theta\right) = k_{44}$

$$\frac{\partial C_1}{\partial \overline{\sigma}} = -m_b\sigma_{ci}\frac{\overline{\sigma}}{\overleftrightarrow{\sigma}}\left(k_{24}+k_{25}\sin 3\theta+k_{26}\sin^2 3\theta\right)=k_{45}$$

$$\frac{\partial C_1}{\partial \theta} = -3m_b\sigma_{ci}\overleftrightarrow{\sigma}(k_{25}\cos 3\theta+k_{26}\sin 6\theta)=k_{46}$$

$$\frac{\partial C_2}{\partial \sigma_m} = -m_b\sigma_{ci}\frac{\overline{\sigma}}{\overleftrightarrow{\sigma}}\left(k_{24}+k_{25}\sin 3\theta+k_{26}\sin^2 3\theta\right) + \frac{3\tan 3\theta}{\overline{\sigma}}m_b\sigma_{ci}\overleftrightarrow{\sigma}(k_{25}\cos 3\theta+k_{26}\sin 6\theta)=k_{27}$$

$$\frac{\partial C_2}{\partial \overline{\sigma}} = -m_b\sigma_{ci}\left(A+B\sin 3\theta+C\sin^2 3\theta\right)\frac{\varepsilon^2}{\overleftrightarrow{\sigma}^3} - \frac{\varepsilon^2}{\overline{\sigma}^2\overleftrightarrow{\sigma}}3\tan 3\theta m_b\sigma_{ci}(B\cos 3\theta+C\sin 6\theta)=k_{28}$$

$$\frac{\partial C_2}{\partial \theta} = 3m_b\sigma_{ci}(B\cos 3\theta+C\sin 6\theta)\left(-\frac{\overline{\sigma}}{\overleftrightarrow{\sigma}}+3\frac{\overleftrightarrow{\sigma}}{\overline{\sigma}}\sec^2 3\theta\right) - \frac{9\tan 3\theta}{\overline{\sigma}}m_b\sigma_{ci}\overleftrightarrow{\sigma}(B\sin 3\theta-2C\cos 6\theta)=k_{29}$$

$$\frac{\partial C_3}{\partial \sigma_m} = \frac{3\sqrt{3}m_b\sigma_{ci}\overleftrightarrow{\sigma}(k_{25}+2k_{26}\sin 3\theta)}{2\overline{\sigma}^3}=k_{30}$$

$$\frac{\partial C_3}{\partial \overline{\sigma}} = \frac{3\sqrt{3}m_b\sigma_{ci}(B+2C\sin 3\theta)}{2}\left(\frac{\overline{\sigma}}{\overleftrightarrow{\sigma}}-\frac{3}{\overline{\sigma}^4}\right)=k_{31}$$

$$\frac{\partial C_3}{\partial \theta} = \frac{9\sqrt{3}m_b\sigma_{ci}\overleftrightarrow{\sigma}C\cos 3\theta}{\overline{\sigma}^3}=k_{32}$$

where

$$k_{33} = -16\sin 2\theta_T m_b\sigma_{ci}\left(-\frac{2}{X^3}k_{13}+k_{17}\right) + 1.5\left(\frac{2k_{13}k_{14}k_{17}+k_{13}^2-16\sin 2\theta_T m_b\sigma_{ci}}{X^3}-\frac{3k_{14}k_{13}^3}{X^4}\right)$$

$$k_{34} = \frac{k_{13}^3}{X^2}-\frac{2k_{13}k_{17}}{X};$$

$$k_{35} = k_{16}\sin 2\theta_T+2(k_{13}^2+Yk_{17})\sin^2\theta_T+k_{33}\cos^2\theta_T+k_{34}\sin 2\theta_T$$

$$k_{36} = -\frac{2m_b\sigma_{ci}k_{13}}{Y^3}-\frac{2Pk_{17}}{Y^3}+\frac{6Pk_{13}^2}{Y^4};\quad k_{37} = -\frac{3m_b\sigma_{ci}k_{13}}{Y^4}-\frac{3Pk_{17}}{Y^4}+\frac{12Pk_{13}^2}{Y^5}$$

$$k_{38} = 2(Z\cos\theta_T+2Y\langle\psi\rangle\sin\theta_T)(k_{16}\cos\theta_T+2k_{17}\langle\psi\rangle\sin\theta_T) + 2(k_{15}\cos\theta_T+2k_{13}\langle\psi\rangle\sin\theta_T)^2$$

$$k_{39} = \frac{8}{9m_b\sigma_{ci}}\left(2k_{18}k_{19}+k_{10}k_{36}-4k_{20}k_{21}+\frac{Pk_{35}}{Y^2}-\frac{2Pk_{38}}{Y^3} -2(Z\cos\theta_T+2Y\langle\psi\rangle\sin\theta_T)^2k_{37}\right)$$

$$k_{40} = -\frac{8\cos\theta_T}{3m_b\sigma_{ci}}(2k_{19}(k_{15}\cos\theta_T+2k_{13}\langle\psi\rangle\sin\theta_T) +(Z\cos\theta_T+2Y\langle\psi\rangle\sin\theta_T)k_{36}+\frac{P(k_{16}\cos\theta_T+2k_{17}\langle\psi\rangle\sin\theta_T)}{Y^2}\right)$$

$$k_{41} = \frac{\partial^2 A}{\partial\sigma_m^2} = -\frac{8\cos^2\theta_T}{3m_b\sigma_{ci}}\left(\frac{m_b\sigma_{ci}k_{13}}{Y^2}+k_{13}k_{19}+\frac{Pk_{17}}{Y^2}\right) - \left(\frac{\cos 6\theta_T\sin 3\theta_T}{\cos^3 3\theta_T}+0.5\tan^3 3\theta_T\right)k_{40}+1.5\tan^2 3\theta_T k_{39}$$

$$k_{42} = \frac{\partial^2 B}{\partial\sigma_m^2} = \sec^3 3\theta_T(k_{40}\cos 6\theta_T-0.5k_{39}\langle\psi\rangle\sin 6\theta_T)$$

$$k_{43} = \frac{\partial^2 C}{\partial\sigma_m^2} = 0.5\sec^3 3\theta_T(k_{40}\langle\psi\rangle\tan 3\theta_T-k_{39})$$

$$k_{47} = \frac{-\sqrt{3}}{2\cos 3\theta\overline{\sigma}^3};\quad k_{48} = \frac{3\sqrt{3}J_3}{2\cos 3\theta\overline{\sigma}^4}$$

(i) For $|\theta| < \theta_T$,

$$\begin{aligned}\nabla^2 f &= \frac{\partial C_2}{\partial\boldsymbol{\sigma}}\frac{\partial\overline{\sigma}}{\partial\boldsymbol{\sigma}}+C_2\frac{\partial^2\overline{\sigma}}{\partial\boldsymbol{\sigma}^2}+\frac{\partial C_3}{\partial\boldsymbol{\sigma}}\frac{\partial J_3}{\partial\boldsymbol{\sigma}}+C_3\frac{\partial^2 J_3}{\partial\boldsymbol{\sigma}^2}\\ &= (k_6+k_7k_{48})\frac{\partial\overline{\sigma}}{\partial\boldsymbol{\sigma}}\otimes\frac{\partial\overline{\sigma}}{\partial\boldsymbol{\sigma}}+k_7k_{47}\frac{\partial J_3}{\partial\boldsymbol{\sigma}}\otimes\frac{\partial\overline{\sigma}}{\partial\boldsymbol{\sigma}}\\ &\quad+(k_8+k_9k_{48})\frac{\partial\overline{\sigma}}{\partial\boldsymbol{\sigma}}\otimes\frac{\partial J_3}{\partial\boldsymbol{\sigma}}+k_9k_{47}\frac{\partial J_3}{\partial\boldsymbol{\sigma}}\otimes\frac{\partial J_3}{\partial\boldsymbol{\sigma}}\end{aligned}$$

(ii) For $|\theta| \geqslant \theta_T$,

$$\begin{aligned}\nabla^2 f &= \frac{\partial C_1}{\partial\boldsymbol{\sigma}}\frac{\partial\sigma_m}{\partial\boldsymbol{\sigma}}+\frac{\partial C_2}{\partial\boldsymbol{\sigma}}\frac{\partial\overline{\sigma}}{\partial\boldsymbol{\sigma}}+C_2\frac{\partial^2\overline{\sigma}}{\partial\boldsymbol{\sigma}^2}+\frac{\partial C_3}{\partial\boldsymbol{\sigma}}\frac{\partial J_3}{\partial\boldsymbol{\sigma}}+C_3\frac{\partial^2 J_3}{\partial\boldsymbol{\sigma}^2}\\ &= k_{44}\frac{\partial\sigma_m}{\partial\boldsymbol{\sigma}}\otimes\frac{\partial\sigma_m}{\partial\boldsymbol{\sigma}}+(k_{45}+k_{46}k_{48})\frac{\partial\overline{\sigma}}{\partial\boldsymbol{\sigma}}\otimes\frac{\partial\sigma_m}{\partial\boldsymbol{\sigma}}\\ &\quad+k_{46}k_{47}\frac{\partial J_3}{\partial\boldsymbol{\sigma}}\otimes\frac{\partial\sigma_m}{\partial\boldsymbol{\sigma}}+C_2\frac{\partial^2\overline{\sigma}}{\partial\boldsymbol{\sigma}^2}+C_3\frac{\partial^2 J_3}{\partial\boldsymbol{\sigma}^2}\\ &\quad+k_{27}\frac{\partial\sigma_m}{\partial\boldsymbol{\sigma}}\otimes\frac{\partial\overline{\sigma}}{\partial\boldsymbol{\sigma}}+(k_{28}+k_{29}k_{48})\frac{\partial\overline{\sigma}}{\partial\boldsymbol{\sigma}}\otimes\frac{\partial\overline{\sigma}}{\partial\boldsymbol{\sigma}}\\ &\quad+k_{29}k_{47}\frac{\partial J_3}{\partial\boldsymbol{\sigma}}\otimes\frac{\partial\overline{\sigma}}{\partial\boldsymbol{\sigma}}+k_{30}\frac{\partial\sigma_m}{\partial\boldsymbol{\sigma}}\otimes\frac{\partial J_3}{\partial\boldsymbol{\sigma}}+(k_{31}+k_{32}k_{48})\frac{\partial\overline{\sigma}}{\partial\boldsymbol{\sigma}}\otimes\frac{\partial J_3}{\partial\boldsymbol{\sigma}}\\ &\quad+k_{32}k_{47}\frac{\partial J_3}{\partial\boldsymbol{\sigma}}\otimes\frac{\partial J_3}{\partial\boldsymbol{\sigma}}\end{aligned}$$

$$\frac{\partial^2 J_3}{\partial\boldsymbol{\sigma}^2} = \frac{1}{3}\begin{bmatrix} s_r-s_z-s_\theta & 2s_\theta & 2\tau_{rz} & 2s_z\\ 2s_\theta & s_r-s_z-s_\theta & 2\tau_{rz} & 2s_r\\ 2\tau_{rz} & 2\tau_{rz} & -6\tau_{rz} & -4\tau_{rz}\\ 2s_z & 2s_r & -4\tau_{rz} & s_r-s_z-s_\theta\end{bmatrix};$$

$$\frac{\partial^2\overline{\sigma}}{\partial\boldsymbol{\sigma}^2} = \frac{1}{\overline{\sigma}}\left[\frac{1}{2}\frac{\partial\boldsymbol{s}}{\partial\boldsymbol{\sigma}}-\frac{\partial\overline{\sigma}}{\partial\boldsymbol{\sigma}}\otimes\frac{\partial\overline{\sigma}}{\partial\boldsymbol{\sigma}}\right]$$

$$\frac{\partial\boldsymbol{s}}{\partial\boldsymbol{\sigma}} = \begin{bmatrix} 2/3 & -1/3 & 0 & -1/3\\ -1/3 & 2/3 & 0 & -1/3\\ 0 & 0 & 2 & 0\\ -1/3 & -1/3 & 0 & 2/3\end{bmatrix};$$

$$\frac{\partial\overline{\sigma}}{\partial\boldsymbol{\sigma}}\otimes\frac{\partial\overline{\sigma}}{\partial\boldsymbol{\sigma}} = \frac{1}{4\overline{\sigma}^2}\begin{bmatrix} s_r^2 & s_rs_z & 2\tau_{rz}s_r & s_rs_\theta\\ s_rs_z & s_z^2 & 2\tau_{rz}s_z & s_zs_\theta\\ 2\tau_{rz}s_r & 2\tau_{rz}s_z & 4\tau_{rz}^2 & 2\tau_{rz}s_\theta\\ s_rs_\theta & s_zs_\theta & 2\tau_{rz}s_\theta & s_\theta^2\end{bmatrix}$$

To avoid division by $\overline{\sigma}$, following equations were been used:

$$\overline{C}_3 = C_3\overline{\sigma}^2 \text{ and } \frac{\overline{\partial J_3}}{\partial\boldsymbol{\sigma}} = \frac{1}{\overline{\sigma}^2}\frac{\partial J_3}{\partial\boldsymbol{\sigma}};\quad \overline{\frac{\partial^2\overline{\sigma}}{\partial\boldsymbol{\sigma}^2}} = \overline{\sigma}\frac{\partial^2\overline{\sigma}}{\partial\boldsymbol{\sigma}^2} \text{ and } \frac{\overline{\partial J_3}}{\partial\boldsymbol{\sigma}} = \frac{1}{\overline{\sigma}}\frac{\partial^2 J_3}{\partial\boldsymbol{\sigma}^2}.$$

References

[1] Hoek E, Brown ET. Empiricatrength criterion for rock masses. J Geotech Eng Div ASCE 1980;106(9):1013–35.

[2] Hoek E, Brown ET. The Hoek–Brown failure criterion – a 1988 update. In: Rock engineering for underground excavations, proc 15th Canadian Rock mech symp. University of Toronto; 1988. p. 31–8.

[3] Hoek E, Brown ET. Practical estimates of rock mass strength. Int J Rock Mech Min Sci 1997;34(8):1165–86.

[4] Hoek E, Carranza-Torres C, Corkum B. Hoek–Brown failure criterion-2002 edition. In: Proceedings of the North American rock mechanics society meeting in Toronto; 2002.

[5] Sakurai S. Back analysis in rock engineering. In: Hudson JA, editor. Comprehensive rock engineering-excavation, support and monitoring, vol. 4. Oxford: Pergamon Press; 1993. p. 543–69.

[6] Martin CD, Maybee WG. The strength of hard-rock pillars. Int J Rock Mech Min Sci 2000;37:1239–46.

[7] Swift GM, Reddish DJ. Underground excavations in rock salt. Geotech Geol Eng 2005;23:17–42.

[8] Serrano A, Olalla C. Ultimate bearing capacity of an anisotropic discontinuous rock mass, part I: basic modes of failure. Int J Rock Mech Min Sci 1998;35(3):301–24.

[9] Serrano A, Olalla C. Ultimate bearing capacity of an anisotropic discontinuous rock mass, part II: determination procedure. Int J Rock Mech Min Sci 1998;35(3):325–48.

[10] Yang XL, Yin JH. Upper bound solution for ultimate bearing capacity with modified Hoek–Brown failure criterion. Int J Rock Mech Min Sci 2005;42:550–60.

[11] Merifield RS, Lyamin AV, Sloan SW. Limit analysis solutions for the bearing capacity of rock masses using the generalised Hoek–Brown yield criterion. Int J Rock Mech Min Sci 2006;43:920–37.

[12] Saada Z, Maghous S, Garnier D. Bearing capacity of shallow foundations on rocks obeying a modified Hoek–Brown failure criterion. Comput Geotech 2008;35:144–54.

[13] You KH, Park YJ, Dawson EM. Stability analysis of jointed/weathered rock slopes using the Hoek–Brown failure criterion. Geosystem Eng 2000;3(3):90–7.

[14] Yang XL, Li L, Yin JH. Stability analysis of rock slopes with a modified Hoek–Brown failure criterion. Int J Numer Anal Methods Geomech 2004;28:181–90.

[15] Li AJ, Merifield RS, Lyamin AV. Stability charts for rock slopes based on the Hoek–Brown failure criterion. Int J Rock Mech Min Sci 2008;45:689–700.

[16] Sloan SW, Booker JR. Removal of singularities in Tresca and Mohr–Coulomb yield functions. Commun Appl Numer Methods 1986;2:173–9.

[17] Krabbenhoft K, Damkilde L. A general non-linear optimization algorithm for lower bound limit analysis. Int J Numer Methods Eng 2003;56:165–84.

[18] Lyamin AV, Yu HS, Sloan SW, Hossain MZ. Lower bound limit analysis for jointed rocks using the Hoek–Brown yield criterion. Austr Geomech 1998:1–17.

[19] Hoek E, Wood D, Shah S. A modified Hoek–Brown criterion for jointed rock masses. In: Hudson JA, editor. Proc rock characterization symp int soc rock mech: Eurock 92. London, Brit Geotech Soc; 1992. p. 209–14.

[20] Nayak GC, Zienkiewicz OC. Convenient form of stress invariants for plasticity. J Struct Div ASCE 1972;98:949–54.

[21] Chakraborty M, Kumar J. Lower bound axisymmetric formulation for geomechanics problems using nonlinear optimization. Int J Geomech 2014 [ISSN 1532-3641/060].

[22] Taiebat HA, Carter JP. Flow rule effects in the Tresca model. Comput Geotech 2008;35:500–3.

[23] Kumar J, Khatri VN. Bearing capacity factors of circular foundations for a general $c-\phi$ soil using lower bound finite elements limit analysis. Int J Numer Anal Methods Geomech 2011;35:393–405.

[24] Sloan SW. Lower bound limit analysis using finite elements and linear programming. Int J Numer Anal Methods Geomech 1988;12:61–77.

[25] Lyamin AV, Sloan SW. Lower bound limit analysis using non-linear programming. Int J Numer Methods Eng 2002;55:573–611.